

Available online at www.sciencedirect.com

SCIENCE @ DIRECT®

Journal of Hydrology xx (xxxx) 1–15

 Journal
of
Hydrology

www.elsevier.com/locate/jhydrol

Investigation of the hydrodynamics of flash floods in ephemeral channels: Scaling analysis and simulation using a shock-capturing flow model incorporating the effects of transmission losses

Simon Marius Mudd *

*Department Of Civil and Environmental Engineering, Vanderbilt University, VU Station B 351831,
2301 Vanderbilt Place Nashville, TN 37235, USA*

Received 21 April 2005; revised 29 August 2005; accepted 11 September 2005

Abstract

Flow and infiltration during flash floods in ephemeral channels were investigated through scaling analysis and numerical experiments. Scaling of the equations governing flow has shown that momentum loss due to transmission losses (flow that infiltrates through the channel bed) during flash floods can be of the same order as momentum loss due to channel friction and can significantly affect the flow velocity. Numerical simulations were carried out using a shock-capturing MUSCL (monotonic upstream-centered scheme for conservation laws), which incorporates transmission losses as a sink term in the momentum and continuity equations. The wetted area of the channel bed during floods is the primary control on the volume of water that can infiltrate into the bed. The increased velocity of floods in narrow channels that adds wetted area to the channel bed due to greater flood propagation distance is not sufficient to overcome the reduction in wetted area due to reduced channel width; wider channels transmit a greater percentage of the flood volume that enters the channel reach to the bed sediments. Floods of the same total volume but different hydrograph shapes transmit different proportions of their volume to the bed sediments; the nature and magnitude of the differences will depend on the flood propagation distance. Increasing the total volume of the flood and decreasing the channel width increases the sensitivity of the total infiltration to the hydrograph shape. For reaches of the same bed area but different spatial distributions of channel width, differences in the rate of channel widening affect the spatial distribution but not the total volume of water that infiltrates into the bed sediments.

© 2005 Published by Elsevier B.V.

Keywords: Ephemeral channels; Flash floods; Scaling analysis; Transmission losses; Numerical modeling

1. Introduction

Flash floods in ephemeral channels are an important component of the hydrologic cycle in arid regions. Precipitation events in arid regions are typically of high intensity yet are spatially localized (Osborn and Lane, 1969; Sharon and Kutiel, 1986;

* Corresponding author. Tel.: +1 615 322 7445; fax: +1 615 322 2138.

E-mail address: simon.m.mudd@vanderbilt.edu

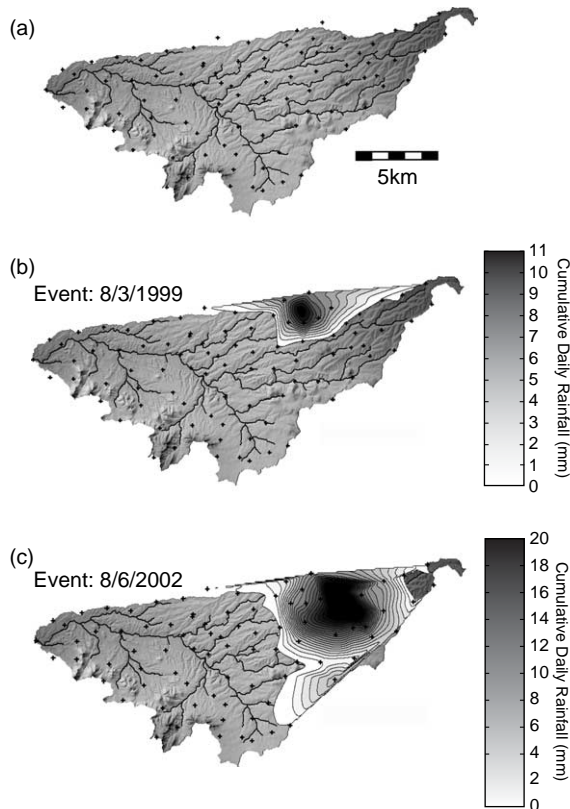


Fig. 1. (a) Shaded relief map of Walnut Gulch Watershed in Arizona showing channel network (solid lines) and raingages (+ symbols). (b), (c) Two examples of localized rainfall events in the Walnut Gulch experimental watershed in Arizona that generated runoff.

Sorman and Abdulrazzak, 1993) (Fig. 1), and floods moving downstream through the channel network can propagate away from the area of runoff generation and over unsaturated bed sediments. During flash floods, water infiltrates into the sediment that makes up the channel bed, and the infiltrated volume can be a significant portion of the total runoff volume (Keppel and Renard, 1962; Lane, 1983). These losses of water to the channel bed, called transmission losses, are an important source of groundwater recharge in arid and semiarid regions (Abdulrazzak and Morel-Seytoux, 1983; Goodrich et al., 2004; Izbicki, 2002; Sorman and Abdulrazzak, 1983; Shentsis and Rosenthal, 2003).

Many factors can affect the spatial distribution of transmission losses and groundwater recharge. Spatial changes in the underlying bedrock can lead to

variation in the ability of transmission losses to recharge groundwater aquifers (Shentsis and Rosenthal, 2003). The depth to groundwater and the thickness of alluvial fill underlying the channel also vary spatially, and affect groundwater recharge and storage. The transmission loss rate has been shown to be reduced when water moving through the vadose zone makes contact with the groundwater table (Abdulrazzak and Morel-Seytoux, 1983). Because of this effect, groundwater pumping near ephemeral channels has been shown to enhance recharge from flow events (Shentsis, 2003). In addition, the porosity and permeability of channel bed sediments may vary spatially along ephemeral channels in the downstream, cross-stream, and vertical dimensions (e.g. Blasch et al., 2004). In many ephemeral channels, a layer of fines is found in the pores of the upper few centimeters of bed sediments; these fines reduce the hydraulic conductivity of the channel bed (e.g. El-Hames and Richards, 1998).

Predicting recharge and maximizing the amount of recharge through pumping requires knowledge of the spatial distribution of transmission losses along the channel, and because of spatial changes in potential recharge, correctly predicting the timing and travel distance of flood events is an essential component of making such predictions. The width of the channel also plays an important role in determining transmission losses, as wider channels have greater total infiltration rates, which increases the potential for channel transmission losses (Goodrich et al., 1997). Goodrich et al. (1997) have shown that transmission losses are also responsible for the strong nonlinearity in basin runoff response from semiarid basins.

Previous studies have investigated the interaction of surface flows and infiltration. Freyberg (1983) studied the effect of a time-varying hydrograph on the infiltration of floodwaters into channel bed sediments in a simulated one-dimensional sediment column. The total volume infiltrated was found to be the same for equal area hydrographs with different peak times but of the same duration. Parissopoulos and Wheeler (1991) extended this analysis with a two-dimensional infiltration model, and found that although hydrographs of equal area and duration but different peak times had the same total infiltration volume, hydrographs of equal area but different duration had large differences in the total infiltrated volume of water.

193 The duration of flow at a particular location in the
194 channel network depends on the velocity and size of
195 the flood, which are affected by the hydrodynamics of
196 the flow and the cumulative transmission losses
197 upstream of that location.

198 A number of studies have combined flow behavior
199 and transmission losses. One branch of this research
200 has studied the problem of an advancing flow front
201 with infiltration in irrigation borders or furrows. Three
202 classes of model for this problem are commonly
203 presented: kinematic, zero-inertia, and full dynamic
204 models. Both kinematic (e.g. Sherman and Singh,
205 1982) and zero-inertia models (e.g. Strelkoff and
206 Katopodes, 1977) make the assumption that the
207 acceleration terms in the momentum equation are
208 negligible. Kinematic solutions also assume the water
209 surface slope is equal to the bottom slope. These
210 assumptions may be appropriate for border irrigation
211 problems because flows in borders systems do not
212 have rapid variations in flow depth and their Froude
213 numbers are typically below 0.3 (Clemmens and
214 Fangmeier, 1978). In the modeling of flash floods,
215 however, these assumptions are inappropriate because
216 in flash floods, the surface depth varies rapidly and
217 Froude numbers are typically near unity (Dick et al.,
218 1997). Full dynamic models combine the full Saint-
219 Venant flow equations with an infiltration model (e.g.
220 Tabuada et al., 1995), and are better suited for
221 describing flow in natural channels than kinematic
222 and zero-inertia models. Due to the fact that irrigation
223 furrows and borders are engineered structures,
224 however, the study of flow and infiltration in such
225 structures has not explored factors important for the
226 prediction of flow and transmission losses in natural
227 channels, such as downstream changes in channel
228 geometry and variations in hydrograph shape. Studies
229 of irrigation furrows focus on length scales of tens to
230 hundreds of meters, whereas floods in ephemeral
231 channels can travel many kilometers.

232 Models that are better suited to the prediction of
233 flow in natural channels include distributed hydro-
234 logic models with channel routing components such
235 as KINEROS (Smith et al., 1995) and the model of
236 El-Hames and Richards (1998). KINEROS has
237 proven to be effective at predicting runoff at the
238 basin scale, but it incorporates a kinematic channel
239 flow model and is not designed to be used in high-
240 resolution investigations of flash flood physics.

241 El-Hames and Richards (1998) use the full Saint-
242 Venant equations to model flow, which are solved
243 with a Lax–Wendroff scheme. The Lax–Wendroff
244 scheme has the disadvantage, shared by the flow
245 routing schemes in full dynamic border irrigation
246 models (e.g. Bautista and Wallender, 1992; Dholakia
247 et al., 1998; Sakkas et al., 1994; Tabuada et al., 1995),
248 that it does not capture flow discontinuities. The
249 leading edge of flash floods in ephemeral channels
250 typically has a steep walled nose, or ‘bore’ (Leopold
251 and Miller, 1956); this bore is a flow discontinuity and
252 is similar to the front of a dam-break flood. Correctly
253 modeling the flood bore is important for flash floods
254 because there is a strong correlation with the size of
255 the flow peak (typically occurring just behind the
256 arrival of the bore) and the velocity of the flood wave
257 (Benzvi et al., 1991; Pilgrim, 1976). Numerical
258 schemes that are not shock capturing also tend to
259 have significant mass balance errors when solving
260 flow problems with discontinuities (Garcia-Navarro
261 et al., 1999).

262 This contribution consists of two components.
263 First, a scaling analysis was performed to assess the
264 significance of transmission losses on a flood’s mass
265 balance and the significance of the source terms (bed
266 slope, channel friction, changes in channel geometry,
267 and transmission loss) on the momentum equation. A
268 numerical model was then developed that couples the
269 one-dimensional Saint-Venant equations and the
270 Richards’ equation. The model solves the Saint-
271 Venant equations using a modified MUSCL (mono-
272 tonic upstream-centered scheme for conservation
273 laws) initially introduced by Vanleer (1979) and
274 solves the Richard’s equation using the scheme of
275 Celia et al. (1990). The numerical simulations
276 performed using the model have focused on a
277 simplified channel in order to isolate the effects of
278 varying channel width, varying cumulative flood
279 volumes, and varying inflow hydrographs on the
280 spatial distribution of transmission losses and down-
281 stream propagation of the flood wave. The work of
282 Freyberg (1983); Parissopoulos and Wheeler (1991) is
283 extended to include feedbacks between surface flow
284 and infiltration in the downstream direction. No
285 attempt is made to predict runoff based on rainfall
286 records, which is a task better suited for distributed
287 models (e.g. Smith et al., 1995; El-Hames and
288 Richards, 1998). Rather, the floods simulated in this

289 study extend the investigations of flows in irrigation
 290 furrows to a scale appropriate for flash floods in
 291 ephemeral channels, and the model is able to simulate
 292 the flood bore by using a shock-capturing numerical
 293 scheme.

294
 295
 296
 297 **2. Scaling analysis of the one-dimensional**
 298 **Saint-Venant equations with infiltration**

299 The Saint-Venant equations are:

300
 301
 302
$$\frac{\partial A}{\partial t} + \frac{\partial Q}{\partial x} = q_l \quad (1a)$$

303 and

304
 305
 306
$$\frac{\partial Q}{\partial t} + \frac{\partial}{\partial x} \left(\frac{Q^2}{A} + gI \right)$$

 307
 308
$$= F_c + gA(S_0 + S_f) + Vq_l, \quad (1b)$$

309 where A is the cross sectional area of flow (L^2), Q is
 310 the discharge (L^3T^{-1}), q_l is the inflow or outflow per
 311 unit length of channel (L^2T^{-1}), g is gravitational
 312 acceleration (LT^{-2}), I is a hydrostatic pressure term
 313 (L^3), F_c is a component of the hydrostatic force in the
 314 x-direction by the channel walls (L^3T^{-2}), S_0 is the
 315 channel slope (dimensionless), S_f is the friction slope
 316 (dimensionless), and $V=Q/A$ is the flow velocity
 317 (LT^{-1}). The hydrostatic pressure term is defined as

318
 319
 320
 321
$$I = \int_0^h (h - \eta)b(\eta)d\eta, \quad (2)$$

322 where h is the flow depth (L), η is an integration
 323 variable indicating distance from the channel bottom
 324 (L), and b is the channel width as a function of
 325 distance above the bed (L). In a rectangular channel b
 326 does not vary with η and the pressure term is:

327
 328
 329
 330
$$I = \frac{A^2}{2b}. \quad (3)$$

331 The component of the hydrostatic force can be
 332 estimated by (Garcia-Navarro, 1999):

333
 334
 335
$$F_c = \frac{g}{\Delta x} (I(h, x + \Delta x) - I(h, x)). \quad (4)$$

336 For a rectangular channel, this can be stated as: 337

338
 339
$$F_c = \frac{gh^2}{2} \frac{\partial b}{\partial x}. \quad (5)$$

340 The friction slope term can be calculated using a
 341 number of flow resistance equations, such as the
 342 Manning equation, Chezy equation, or Darcy–
 343 Weisbach equation. The Darcy–Weisbach equation
 344 was used for this study because it is dimensionally
 345 correct and has a sounder theoretical basis (Channels,
 346 1963). The friction slope calculated with the Darcy–
 347 Weisbach equation is:

348
 349
 350
$$S_f = \frac{ffV^2}{8gR}, \quad (6)$$

351 where ff is the Darcy–Weisbach friction coefficient
 352 (dimensionless) and R is the hydraulic radius (L). For
 353 a rectangular channel, the hydraulic radius is:

354
 355
 356
$$R = \frac{Ab}{2A + b^2}. \quad (7)$$

357 If there are no tributaries, the inflow and outflow
 358 term will consist only of the transmission losses:

359
 360
$$q_l = -f_c b, \quad (8)$$

361 where f_c is the volumetric infiltration rate per unit area
 362 into the bed ($L^3T^{-1}L^{-2}$). The infiltration rate is
 363 defined as positive for infiltration and negative for
 364 exfiltration. The one-dimensional equations for flow
 365 in a rectangular channel become:

366
 367
 368
$$\frac{\partial}{\partial t} (hb) + \frac{\partial}{\partial x} (Vhb) = -f_c b \quad (9a)$$

369 and

370
 371
 372
$$\frac{\partial}{\partial t} (hbV) + \frac{\partial}{\partial x} \left(hbV^2 + \frac{gh^2b}{2} \right)$$

 373
 374
$$= \frac{gh^2}{2} \frac{\partial b}{\partial x} + ghb \left(S_0 + \frac{ffV^2}{8gR} \right) - Vbf_c. \quad (9b)$$

375 Eqs. (9a,b) may be nondimensionalized as follows: 376

377
 378
 379
 380
$$x_* = \frac{x}{X}, \quad t_* = \frac{\sqrt{gh}}{X} t, \quad h_* = h\bar{h},$$

 381
 382
$$b_* = b\bar{b}, \quad V_* = \frac{V}{\sqrt{gh}}, \quad f_* = \frac{f_c}{\theta_f K_s}, \quad (10)$$

 383
 384

where K_s is the saturated hydraulic conductivity of the bed sediments (LT^{-1}), the subscript* indicates a dimensionless quantity, and overbars indicate an averaged quantity. The parameters X and θ_f are dynamic scaling parameters. The parameter X represents the distance from the flood bore, and θ_f is a dimensionless parameter that is greater than or equal to one and scales the saturated hydraulic conductivity. Dynamic scaling for the infiltration is chosen because initial infiltration rates into dry soil columns can be several orders of magnitude greater than infiltration rates into saturated columns. It should be noted that this analysis considers only flash floods contained within the channel walls; floodplain inundation is not considered. The velocity is scaled at the speed of a gravity wave at the average depth of flow in the flood event, and the time is scaled by the time it takes a gravity wave to traverse a distance X . These parameters are adopted because typical flash floods travel at speeds near the critical Froude number (Dick et al., 1997). Flows during border irrigation advance typically travel at a Froude numbers of <0.3 (Clemmens and Fangmeier, 1978), thus for border irrigation advance the dimensionless velocity is $O(10^{-1}-10^0)$.

The dimensionless continuity equation is:

$$\frac{\partial}{\partial t_*}(h_* b_*) + \frac{\partial}{\partial x_*}(V_* h_* b_*) = -\frac{X\theta_f K_s}{\bar{h}\sqrt{gh}} f_* b_* \quad (11)$$

Transmission losses will become a first order contribution to the mass balance when the dimensionless group to the right of the equality of Eq. (11) approaches unity. The dynamic length scale, X , can be adjusted to determine the length of channel which must be swept by the flood before infiltration becomes significant. Consider a typical flash flood in which the average flow depth is $O(10^{-1}-10^0)$. Sandy sediments will have K_s values of $\sim 1 \times 10^{-4}$ m/s. Near the flood bore, where X is $O(10^{-1}$ m), water will infiltrate rapidly due to the suction within the pores of the bed sediments, and θ_f is $O(10^2)$. The contribution of infiltration will be significant to second order (the dimensionless group to the right of the equality in Eq. (11) will approach 0.1) in the total mass balance near the bore for floods with small ($O 10^{-2}-10^{-1}$ m) flow depths or floods taking place in channels with sandy beds. At intermediate length scales (X is

$O(10-1000$ m)), θ_f will approach unity and the infiltration term becomes second order or smaller. At longer length scales, such as the length of a mesoscale drainage basin $O(10$ km), transmission losses become a first order influence on the mass balance. A silt-clogging layer in the bed sediments can reduce the saturated hydraulic conductivity by an order of magnitude (El-Hames and Richards, 1998); for floods over bed sediments containing a clogging layer of fines, the flood propagation distance must be greater for infiltration to be significant than in the case of channels whose beds are not clogged with fines.

The dimensionless momentum equation is:

$$\begin{aligned} \frac{\partial}{\partial t_*}(h_* b_* V_*) + \frac{\partial}{\partial x_*}(h_* b_* V_*^2) + \frac{1}{2} \frac{\partial}{\partial x_*}(h_*^2 b_*) \\ = \frac{h_*^2}{2} \frac{\partial b}{\partial x_*} + X S_0 \bar{h} h_* b_* \\ + X f f \left(\frac{h_*}{4b} + \frac{b_*}{8h} \right) V_*^2 - \frac{X\theta_f K_s}{\sqrt{gh}} V_* b_* f_* \end{aligned} \quad (12)$$

The hydrostatic force term due to channel width changes is always first order. Other source terms can vary significantly depending on the dynamic length scale, the friction factor, and the value of θ_f . The slope term (second term on the left) will only be of first order significance at the basin scale. The friction slope term can be significant at the basin scale, but can also be significant at the nose of the flood bore. Experimental results have shown that friction increases as a function of the ratio between D_{84} and R (Abdulrazzak and Morel-Seytoux, 1983, p.102, and references therein). In the analytical solution of a dam-break, flow over a frictionless dry bed the flood wave will spread to a thin sheet on the advancing side of the flood (Henderson, 1966). In the case of a natural channel with channel friction, the thinning of flow near the advancing end of a flood will cause a greater amount of resistance as R decreases, and a steep front will develop. The Manning equation predicts greater resistance in flows that are shallow, but will under-predict the friction force near the bore due to the fact that it does not account for the change in the friction factor as R becomes small. The Darcy–Weisbach friction equation includes the relationship between the hydraulic radius, R , and the channel roughness, which

can be quantified by $D_{84}(L)$:

$$\frac{1}{\sqrt{ff}} = 0.82 \log \left(4.35 \frac{R}{D_{84}} \right). \quad (13)$$

The friction term thus can be of first order significance at the nose of the bore where the friction factor is large ($O 10^0-10^1$).

Similarly, the momentum loss due to transmission losses can be significant at the basin scale and near the bore. At basin scale, θ_f is ~ 1 , but X is large. The collective momentum loss due to transmission losses over a basin will significantly slow the passage of the flood compared to a flood that does not experience transmission losses. This result shows that in order to properly predict flood travel times in ephemeral channels at the basin scale the momentum loss due to transmission losses must be incorporated into the flood routing scheme. Near the bore, X is small but θ_f is large, so the momentum loss due to transmission losses is also significant near the bore. This momentum loss, in addition to the increased friction near the bore, is the cause of the characteristic steep front of a flash flood bore. This steep front is an important feature of flash floods in ephemeral channels because it has been theorized that elevated turbulence and friction in the bore is responsible for the high suspended and bedload sediment concentrations measured during flash flood events (Dunkerley and Brown, 1999; Laronne and Reid, 1993).

3. Coupled shock-capturing open channel flow and infiltration model

A model that couples the infiltration of water into the channel bed sediment and the flow of the flood in the channel has been developed. This model consists of an infiltration component and a channel flow component; these components are coupled through the source terms in the continuity and momentum equations for channelized flow.

3.1. Infiltration component

Each channel node in the model is underlain by a one-dimensional sediment column. For each column, the model calculates infiltration (f_c in Eqs. (9a,b)) by

solving the mixed form of the Richard's equation

$$\frac{\partial \theta}{\partial t} - \nabla \cdot K(h_p) \nabla h_p - \frac{\partial K}{\partial z} = 0, \quad (14)$$

where $K(h_p)$ is the unsaturated hydraulic conductivity (LT^{-1}) (a function of the pressure head), θ is the moisture content (L^3L^{-3}), and h_p is the pressure head (L). The hydraulic conductivity and moisture content are both functions of the pressure head, and are determined by the van Genuchten constitutive equations (van Genuchten, 1980). Eq. (14) is solved using a finite difference spatial approximation of the modified Picard iterative technique introduced by Celia et al. (1990). Sediment columns are of sufficient depth to prevent the wetting front from interacting with the lower boundary of the columns. For simplicity, lateral flow in the vadose zone is not considered.

3.2. Channel flow component

The model solves the Saint-Venant equations using a modified MUSCL scheme. The scheme presented here calculates flux terms analogously to the third order scheme presented by Delis and Skeels (1998) but differs in its treatment of the source terms in Eqs. (1a,b). Instead of the Manning equation, the model used in this study uses the Darcy–Weisbach equation for the friction slope for reasons described in Section 2. The model solves the term F_c in Eq. (1b) using the method of Garcia-Navarro et al. (1999). The MUSCL scheme presented by Delis and Skeels (1998) can accurately capture the solution of a dam-break flow over a dry bed in the case of a frictionless channel, but including friction can lead to instabilities as extremely high frictions are introduced at the downstream edge of the flood. The current model corrects these instabilities by using a two-step procedure. The model calculates predicted values of the flow area and discharge at the future timestep using a solution of the Saint-Venant equations that excludes source terms due to friction and transmission losses. These predicted values of A and Q at the i th node are then averaged with the values at the old timestep:

$$A_i^a = \frac{A_i^p + A_i^t}{2}, \quad (15a)$$

$$Q_i^a = \frac{Q_i^p + Q_i^t}{2}, \quad (15b)$$

where the superscripts a, p, and t indicate average, predictor, and previous timestep, respectively. The head boundary at the surface of the bed sediment is determined by the flow depth calculated from the averaged channel area (A_i^a). The friction slope is also calculated using the averaged channel area (A_i^a) and discharge (Q_i^a), and then using the averaged source terms the values of A_i and Q_i at the future timestep are calculated using the full Saint-Venant equations including the frictional terms. An inflow discharge hydrograph is used as the upstream boundary condition. The velocity and flow depth at this boundary is then calculated using the method described in Garcia-Navarro and Saviron (1992). The downstream boundary is set as having a discharge of zero at all times; the simulations are run with a channel length and flood duration such that the flood bore never reaches the downstream boundary.

4. Numerical experiments

Here the results from a series of numerical experiments are presented. For illustrative purposes, the temporal response of the infiltration rate into a column of sediment due to ponding of water on the surface is described. Results of a series of experiments using the coupled flow and infiltration model are then presented. In natural channels, there are numerous factors, which influence both the propagation rate of the flood and the rate and spatial distribution of transmission losses. Factors affecting the rate of propagation of the flood can include channel sinuosity, downstream changes in the channel cross section (e.g. Garcia-Navarro et al., 1999), and lateral inflows of water from hillslopes and tributary drainage basins (e.g. Shentsis et al., 1999). Transmission losses can also be affected by the complex stratigraphy of channel bed sediments (e.g. Blasch et al., 2004). The combination of these factors makes it difficult to isolate controls on transmission losses and downstream flood propagation using data from natural watersheds. In addition, it is common for flow-recording instruments in ephemeral channels to be positioned in such a way that lateral inflow occurs between instrumented

sites (e.g. Shentsis et al., 1999). Such a positioning of instruments, while useful in assessing the basin scale water balance, nonetheless makes it difficult to assess the physics of floods as they travel between instrumented cross sections. In order to isolate the effects of varying the channel width, the total flood volume, inflow hydrograph, and the bed geometry on transmission losses we simulate a simplified channel in which only one parameter is varied for a set of simulations. In this way, the numerical model serves as a virtual laboratory (e.g. Bras et al., 2003) for exploring the interaction of floods and transmission losses. The simulations focus on flash floods that are contained within the channel banks; large floods that inundate the floodplain are not considered.

4.1. Infiltration into a single sediment column

To begin to understand how infiltration affects and is affected by a propagating flash flood hydrograph, one can first examine infiltration in sediment overlain by ponded water. As water depth at the sediment surface increases, infiltration also increases (Fig. 2(a)). The sensitivity of the total infiltration decreases with increasing surface water depth. For large surface water depth, changes in the depth of the water at the surface do not significantly affect the total infiltration compared with the total infiltration for small surface water depths.

Fig. 2(b) shows infiltration curves for two different depths of surface water (sediment properties are shown in Table 1). The infiltration rate is initially high and then decays to a value that is a function of the saturated hydraulic conductivity and the water depth at the sediment's surface. The curves in Fig. 2(b) have a constant depth of surface water as the upper boundary condition, but in the case of a flash flood, the flow depth will vary rapidly. The infiltration curves for sediment with a rapidly varying surface depth will be perturbed versions of the exponential decay curves shown in Fig. 2(b) (for example, see Fig. 13 in Freyberg, 1983). Infiltration rates into initially dry sediment at the onset of ponding can be one to two orders of magnitude greater than the steady state infiltration rate. The infiltration rate in a sandy soil ($K_{\text{sat}} = 9.22 \times 10^{-5}$ m/s) with a surface water depth of 0.50 m at time = 1 s is 4.8×10^{-3} m/s. This high infiltration rate rapidly decays (within tens

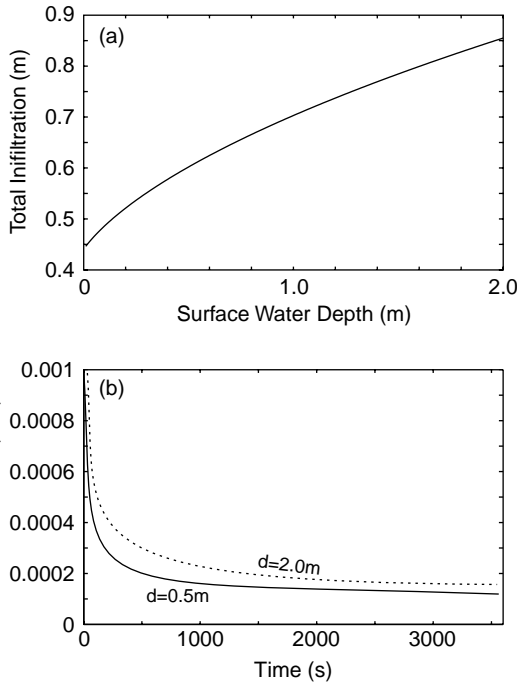


Fig. 2. (a) Total depth of water infiltrated after one hour as a function of surface water column depth. (b) Infiltration rate as a function of time for different surface water column depths. Sediment properties given in Table 1.

of seconds) to a rate that is of the same order of magnitude as the steady state infiltration rate.

4.2. The effects of channel width and peak inflow discharge

In the first set of simulations using the fully coupled model, both the channel width and the inflow

Table 1 Model parameter values

Parameter	Value
α 0(1/cm)	0.0335
N (dimensionless)	2.0
θ_r (Dimensionless)	0.102
θ_s (Dimensionless)	0.368
K_s (cm/s)	0.00922
K_s (cm/s) of clogging layer	0.001
λ (Dimensionless)	0.5
S_0 (dimensionless)	0.01
Initial pressure head h_{p0} (m)	-5.0
D_{84} (m)	0.0005

discharge are varied. The channel width for each simulated channel does not vary in space. The inflow hydrographs are triangular; they rapidly reach a peak Q_p after 120 s and then decay to zero at time t_{end} (Fig. 3(a)). This is a simplification of a peaked hydrograph typical of many floods (e.g. Fig. 3(b)). For each peak discharge and channel width, floods are modeled both with and without a 5 cm layer of fines near the channel bed surface (the hydraulic conductivity of this clogging layer is listed in Table 1).

First, consider two floods with the same inflow hydrograph but different channel widths. The narrower channels have greater flow depths and a smaller wetted perimeter, resulting in less flow resistance than a flood in a wider channel. This will lead to faster flow velocities. At the same time, the greater flow depths will cause greater rates of infiltration, which will slow the flow (Eq. (1b)). For the channels modeled here, the decreased flow resistance leading to greater flow velocities outweighs the loss of momentum due to greater infiltration caused by greater flow depths.

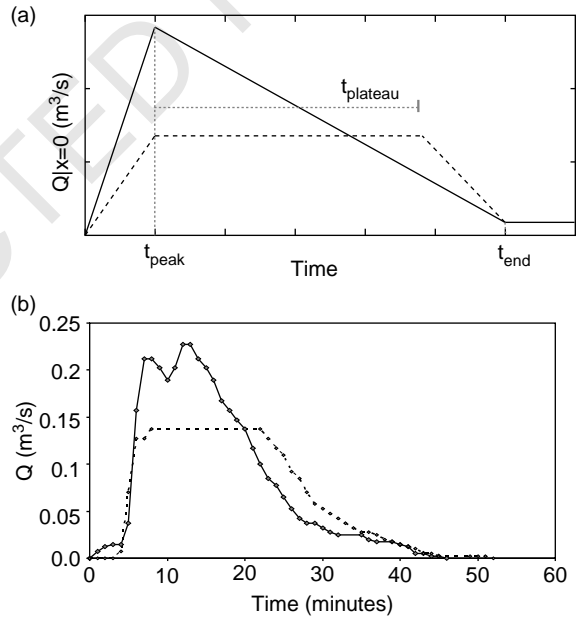
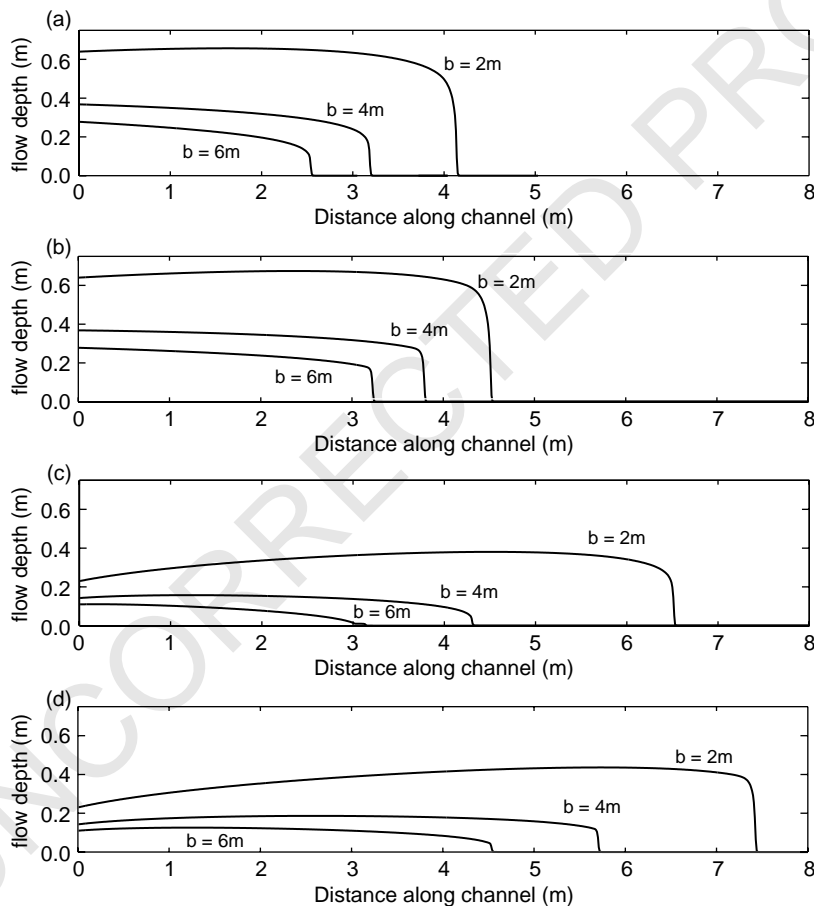


Fig. 3. (a) Inflow flood hydrographs used in simulations. Solid line represents triangular hydrograph, dashed line represents plateau type hydrograph. (b) Two hydrographs from a small basin at the Walnut Gulch Experimental Watershed, AZ (data from flume 3, area = 2220 acres). The dotted line represents a flood that occurred on 9/16/1999, and the solid line represents a flood that occurred on 7/7/1999.

769 Fig. 4 shows the progression of the flood wave for
 770 channels of differing widths, with the narrower
 771 channels having flood waves that propagate at greater
 772 speeds. The clogging layer of fines reduces the
 773 amount of water infiltrated due to the lower hydraulic
 774 conductivity near the channel bed surface. This
 775 reduces the momentum losses associated with
 776 transmission losses (Compare Fig. 4(a) and (b), and
 777 also Fig. 4(c) and (d)). Any reduction in the hydraulic
 778 conductivity of the bed sediments will lead to greater
 779 flood wave celerities.

780 As water infiltrates into the bed, the flood discharge
 781 is reduced. Fig. 5 shows hydrographs at several points
 782 along simulated channels. The volumetric flux rate of
 783 water into the bed sediments within the reach will
 784 depend on both the local infiltration rate at a cross
 785

817 section, as well as the width of the channel and the
 818 distance the flood has traveled (the farther the flood
 819 travels, the more wetted surface area is available for
 820 water to enter the channel substrate). The infiltration
 821 rate will depend on the hydraulic conductivity of the
 822 bed sediments. While Guzman et al. (1989) con-
 823 sidered the increase in infiltration due to an increase in
 824 the wetted surface at a one-dimensional cross section,
 825 and found increasing wetted area increased the
 826 infiltration volume, their work did not consider
 827 the effects of the change in wetted perimeter on the
 828 downstream propagation distance of a flash flood. A
 829 volume ratio, ϕ_V , is defined as the ratio of the total
 830 volume of water infiltrated to the total volume of
 831 water that has passed through the upstream boundary.
 832 For example, if $\phi_V=1$, all of the water that has
 833



815 Fig. 4. Passage of flood waves for floods with $Q_p=4.0 \text{ m}^3 \text{ s}^{-1}$. (a) $t=45 \text{ min}$, no clogging layer. (b) $t=45 \text{ min}$, with clogging layer. (c) $t=$
 816 80 min , no clogging layer, (d) $t=80 \text{ min}$, with clogging layer.

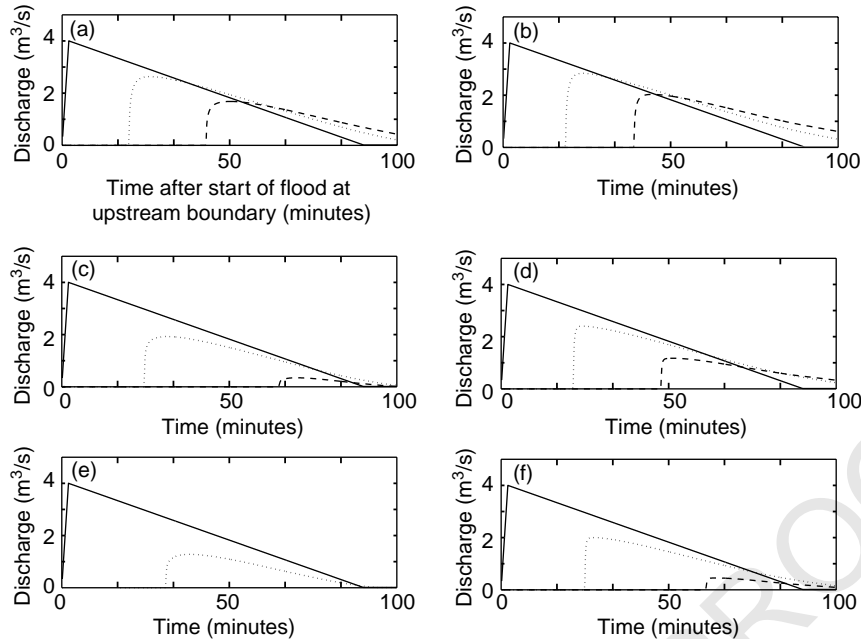


Fig. 5. Hydrographs for floods with $Q_p = 4.0 \text{ m}^3 \text{ s}^{-1}$. Solid line is the inflow hydrograph, dotted line is the hydrograph 2 km from the upstream boundary of the simulated reach, and dashed line is the hydrograph 4 km from the upstream boundary of the simulated reach. (a) $b = 2 \text{ m}$, no clogging layer, (b) $b = 2 \text{ m}$, with clogging layer, (c) $b = 4 \text{ m}$, no clogging layer, (d) $b = 4 \text{ m}$, with clogging layer, (e) $b = 6 \text{ m}$, no clogging layer, (f) $b = 6 \text{ m}$, with clogging layer.

entered the channel has infiltrated into the bed sediments. Volume ratios as a function of time are plotted in Fig. 6. For floods with the same inflow hydrographs, wider channels will result in greater volume ratios at all times during the flood. A clogging layer of fines will reduce the volume ratio for a flood of the same peak inflow discharge and channel width.

Wide channels have greater volumetric flux rates of water into the bed sediment than narrow channels. Although greater flow depths in narrow channels lead to increased infiltration rates per unit width (e.g. Fig. 2(b)), the increase in infiltration with the depth of water in narrow channels is less than the increase in volumetric flux due to the greater area of the channel bed through which infiltrating water can flow in wider channels. Floods in narrow channels also have greater velocities than floods in wide channels, so the length along the channel that is wetted and is therefore experiencing infiltration grows at a greater rate, but the increase in the velocity is not great enough to offset the added wetted area that is due to a wider channel.

In channels of the same width, floods with greater inflow discharge will have lower volume ratios through time than for floods with smaller inflow discharge. As demonstrated in Section 4.1, the infiltration rate becomes insensitive to changes in the flow depth at large flow depths, so the speed and volume ratios in floods with greater discharges, and thus greater flow depths, are less sensitive to infiltration of water into the channel bed sediments.

4.3. The effects of hydrograph shape

Both Freyberg (1983); Parissopoulos and Wheater (1991) found that the total amount of water infiltrated into a channel cross section would be nearly identical for hydrographs of different shape but with the same total volume (e.g. the area under the hydrograph). While the shape of the hydrograph may not play a significant role at a given cross section of channel, it can have an impact upon the distribution and magnitude of infiltration along the channel because the velocity of the flood is sensitive to the discharge, 960

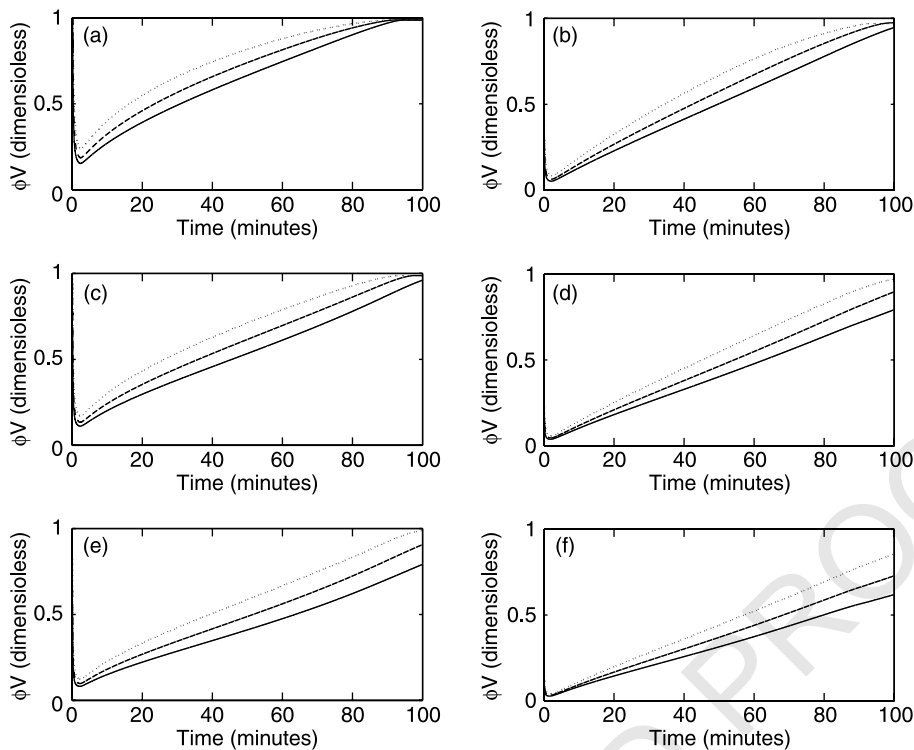


Fig. 6. Volume ratios as a function of time. The solid lines represent floods in channels 4 m wide, dashed lines represent flood in channels that are 6 m wide, and dotted lines represent floods in channels that are 10 m wide. (a) $Q_p = 2.0 \text{ m}^3 \text{ s}^{-1}$, no clogging layer, (b) $Q_p = 2.0 \text{ m}^3 \text{ s}^{-1}$, with clogging layer, (c) $Q_p = 4.0 \text{ m}^3 \text{ s}^{-1}$, no clogging layer, (d) $Q_p = 4.0 \text{ m}^3 \text{ s}^{-1}$, with clogging layer, (e) $Q_p = 8.0 \text{ m}^3 \text{ s}^{-1}$, no clogging layer, (f) $Q_p = 8.0 \text{ m}^3 \text{ s}^{-1}$, with clogging layer.

and as has been demonstrated above, the speed of the flood wave is more important in determining the volume of water that infiltrates into the bed sediments than the depth of flow. Floods of the same total volume of water but with inflow hydrographs of different shapes were simulated. Each set of floods with identical total inflow water volumes was simulated using a triangular and a plateau-like hydrograph (Fig. 3(a)). A plateau-like hydrograph is shown in Fig. 3(b) (flood on 9/16/1999), or see hydrographs from Dick et al. (1997) or Malmon et al. (2004). The plateau-like hydrograph is a simplification used to illustrate the hydrodynamics of floods in which flow volume is distributed more evenly through the hydrograph than in a singly peaked hydrograph. Floods in which the total flow volume is more evenly distributed about the peak discharge could be caused by differing arrival times of flash floods from tributary

channels upstream of a given cross section of channel (e.g. Dick et al., 1997).

For the floods with plateau-like inflow hydrographs, the discharge at the peak is a fraction of the peak of the triangular hydrograph ($\theta_p = Q_{pl}/Q_p$ where Q_{pl} is the discharge of the plateau). For smaller θ_p , the time of the plateau, t_{pl} , will be greater. The progression of three flood waves with the same channel width and total flood volume is shown in Fig. 7. The flood with the triangular inflow hydrograph has the greatest flow velocity during the initial stages of the flood. Floods with plateau-like hydrographs are initially slower due to smaller peak discharge compared to the floods with a triangular hydrograph. Floods with a plateau-like hydrograph may gain speed downstream, however, because a greater volume of flow is delivered to the channel during the period of the plateau relative to the

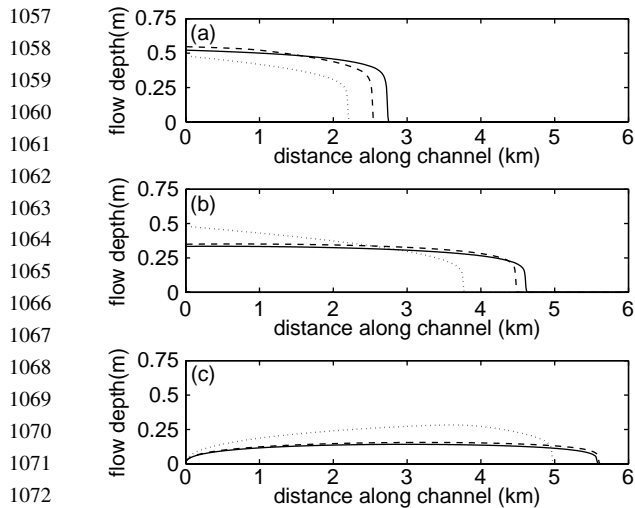


Fig. 7. Passage of flood waves for floods with $Q_p=8.0 \text{ m}^3 \text{ s}^{-1}$, $b=6.0 \text{ m}$. (a) $t=30 \text{ min}$. (b) $t=60 \text{ min}$. (c) $t=90 \text{ min}$. Solid line represents triangular inflow hydrograph. Dashed line has $\theta_p=0.8$, dotted line has $\theta_p=0.6$.

triangular hydrograph. The water delivered during the plateau propagates through the channel after the bed has already been wetted and the infiltration rate has decayed (Fig. 2(b)).

The volume ratios (ϕ_v) of floods with different types of hydrographs are shown in Fig. 8. In the early stages of the flood, the volume ratios for the triangular hydrographs are lower than for the plateau-like hydrographs with the same total volume in channels of the same widths. Although the floods with triangular hydrographs propagate farther down the channel, their discharge early in the flood is greater and the increased wetted area through which water can infiltrate due to their increased propagation distance does not compensate for the increased discharge relative to the floods with plateau-like inflow hydrographs. As time passes, however, more water flows into the channel when the bed is already wet and the infiltration rate has decayed for floods with the plateau-like inflow hydrographs; this leads to lower volume ratios at later times in the floods. Floods of greater total volume and in narrower channels are more sensitive to changes in the hydrograph shape (Fig. 8). After $\sim 80 \text{ min}$ of flow, a flood in a 6 m wide channel with a peak inflow discharge of $4 \text{ m}^3/\text{s}$ can have a volume ratio that is $\sim 25\%$ greater than the

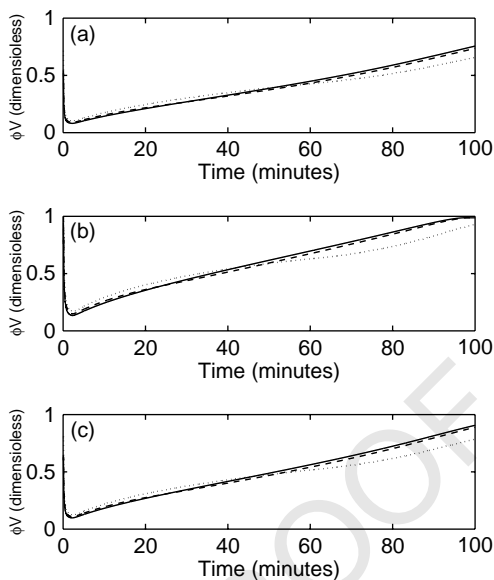


Fig. 8. Volume ratios as a function of time. Solid line represents triangular hydrograph. Dashed line has $\theta_p=0.8$, dotted line has $\theta_p=0.6$. (a) $Q_p=4.0 \text{ m}^3 \text{ s}^{-1}$, $b=2.0 \text{ m}$ (b) $Q_p=4.0 \text{ m}^3 \text{ s}^{-1}$, $b=6.0 \text{ m}$ (c) $Q_p=8.0 \text{ m}^3 \text{ s}^{-1}$, $b=6.0 \text{ m}$.

volume ratio for a flood in the same channel and of the same volume that has a θ_p value of 0.6.

If all of the water during a flash flood infiltrates into the bed sediments, its spatial distribution will be determined by the channel width, the velocity of the flood, and the shape of the hydrograph. It may happen, however, that the flood encounters a perennial stream at a confluence with a larger drainage basin. In such a case, the total volume of water infiltrated is of more concern to the hydrologist studying recharge than the timing of the infiltration. Fig. 9 plots the volume of water infiltrated into the bed once the floods have traveled a given distance. The flood velocity again plays a critical role in determining the total water that infiltrates into the bed sediments. Because the infiltration rate curve (Fig. 2(a)) is relatively insensitive to changes in the flow depth, the time a column of sediment is wetted by the flood is the principal factor that determines the total volume of water that infiltrates. In channels of the same width, floods that travel down the channel at greater speeds will lose the greatest volume of water to the bed after traveling a given distance.

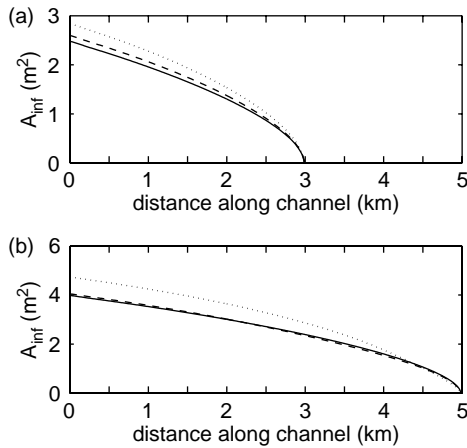


Fig. 9. A_{inf} is the depth of water infiltrated times the channel width. The total volume infiltrated is the area under the curves. Solid line represents triangular hydrograph. Dashed line has $\theta_p=0.8$, dotted line has $\theta_p=0.6$. For all floods $Q_p=8.0\text{ m}^3\text{ s}^{-1}$, $b=6.0\text{ m}$. (a) Floods have traveled 3 km. (b) Floods have traveled 5 km.

4.4. The effects of spatially varying channel width

The geomorphic characteristics of the channel can affect the spatial distribution and rate of infiltration in ephemeral channels. Consider channels that are either uniform (as in the previous model runs), or are widening downstream. Simulations have been

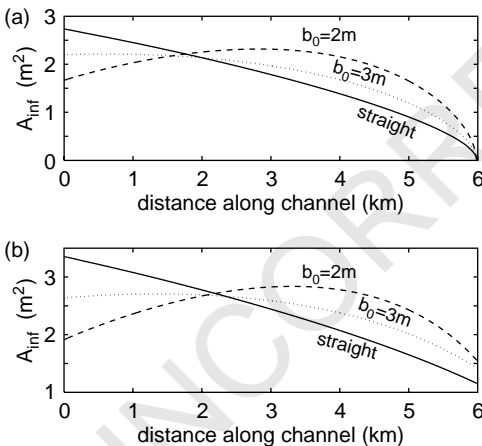


Fig. 10. A_{inf} as in Fig. 7. The uniform channel has a width of 4 m. The parameter b_0 is the width of the channel at the upstream boundary. For all floods $Q_p=8.0\text{ m}^3\text{ s}^{-1}$. The bed area of the channels is the same over the channel length (L) 6 km. (a) A_{inf} for the floods when they reach 6 km. (b) A_{inf} after 90 min.

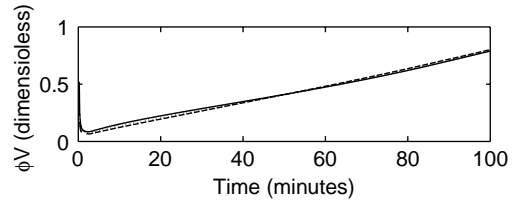


Fig. 11. Characteristic plot of volume ratios as a function of time for channels of different spatial distributions of channel width. Differences in volume ratio are negligible.

performed for channels with constant bed areas in the downstream direction and with channels that have different widths as a function of distance from the upstream boundary of the channel reach. This mimics the channel-widening characteristic of natural channels (e.g. Leopold and Miller, 1956) (although, for simplicity, the widening of the channel as a function of distance is simplified as linear).

Results from one set of runs are shown in Fig. 10. The spatial distribution of the water that has infiltrated into the bed varies strongly with the spatial variation in channel width. Increasing the difference between the width at the upstream boundary of the reach and at $x=L$ leads to decreased volumes of water in the channel near the upstream reach boundary and, in some cases increasing volumes of water that have infiltrated into the bed sediments downstream. While the spatial distribution of the volume of water that has infiltrated into the bed shows strong spatial variations depending on the downstream trend in channel width, the volume ratio is relatively insensitive to the spatial distribution of channel width (Fig. 11).

5. Conclusions

The effects of the interaction between a flood in an ephemeral channel and infiltration into its bed have been investigated. Scaling analysis has been used to demonstrate analytically the findings of field investigators (e.g. Lane, 1983) that infiltration is important in the mass balance of floods in ephemeral channels at the basin scale (on the order of 10 km). The scaling analysis has also shown that infiltration is important in the mass balance near the bore, and plays an important role in the momentum balance of floods in ephemeral channels at the basin scale. Because transmission

1249 losses play an important role in the momentum
1250 balance during flash floods, flood routing schemes
1251 that are used to predict flood velocities and
1252 propagation distances should account for this momen-
1253 tum loss. The momentum losses during flash floods in
1254 ephemeral channels significantly slow floods, which
1255 can give more time for infiltration to occur, but will
1256 result in a lesser area of the channel bed to be wetted.
1257 Numerical simulations have shown that floods of the
1258 same inflow hydrograph but in wider channels have a
1259 greater proportion of their water volume infiltrate into
1260 the bed sediments.

1261 Floods of the same total volume but of different
1262 hydrograph shape will have different proportions of
1263 their total volume infiltrate into the channel bed
1264 sediments. Floods with sharp peaks in their hydro-
1265 graphs will have greater peak flow velocities and
1266 propagate further along the channel than floods with
1267 smoother peaks, leading to a greater wetted area and
1268 more time for the flood waters to infiltrate into the bed
1269 sediments. While hydrograph shape plays an import-
1270 ant role in the proportion of the flood that infiltrated
1271 into the bed, this proportion is relatively insensitive to
1272 changes in channel shape if the total bed area of two
1273 channels is the same. The spatial distribution of
1274 channel width is critical, however, in determining the
1275 spatial distribution of water that infiltrates into the
1276 channel bed.

1277 6. Uncited reference

1280 Knighton, 1998.

1281 Acknowledgements

1282 Field work in Los Alamos, New Mexico that
1283 motivated this study was made possible by Tom
1284 Dunne, Daniel Malmon, the Collaborative UC-Los
1285 Alamos Research (CULAR) program, and the George
1286 Tunnel Memorial Fellowship from the UC Santa
1287 Barbara Department of Geological Sciences. Steve
1288 Reneau and Bob Grey provided assistance and advice
1289 at Los Alamos. H. S. Wheater provided a helpful
1290 review to an earlier version of this manuscript.
1291 Datasets for Fig. 2(b) were provided by the USDA-
1292 ARS Southwest Watershed Research Center. Funding

1297 for these datasets was provided by the United States
1298 Department of Agriculture, Agricultural Research
1299 Service.

1300 References

- 1301 Abdulrazzak, M.J., Morel-Seytoux, H.J., 1983. Recharge from an
1302 ephemeral stream following wetting front arrival to water table.
1303 *Water Resources Research* 19 (1), 194–200.
1304 Bautista, E., Wallender, W.W., 1992. Hydrodynamic furrow
1305 irrigation model with specified steps. *Journal of Irrigation and*
1306 *Drainage Engineering* 118 (3), 450–456.
1307 Benzi, A., Massoth, S., Schick, A.P., 1991. Travel time of runoff
1308 crests in Israel. *Journal of Hydrology* 122 (1–4), 309–320.
1309 Blasch, K., Ferre, T.P.A., Hoffman, J., Pool, D., Bailey, M.,
1310 Cordova, J., 2004. Processes controlling recharge beneath
1311 ephemeral streams. In: Phillips, F.M., Hogan, J.F., Scanlon, B.
1312 (Eds.), *Groundwater Recharge in a Desert Environment: The*
1313 *Southwestern United States*. American Geophysical Union,
1314 Washington, DC, pp. 69–76.
1315 Bras, R.L., Tucker, G.E., Teles, V., 2003. Six myths about
1316 mathematical modeling in geomorphology. In: Wilcock, P.R.,
1317 Iverson, R.M. (Eds.), *Prediction in Geomorphology*. American
1318 Geophysical Union, Washington, DC, pp. 63–79.
1319 Celia, M.A., Bouloutas, E.T., Zarba, R.L., 1990. A general mass-
1320 conservative numerical solution for the unsaturated flow
1321 equation. *Water Resources Research* 26 (7), 1483–1496.
1322 Channels, T.F.o.F.F.i.O., 1963. Friction factors in open channels:
1323 progress report. *Journal of Hydraulic American Society of Civil*
1324 *Engineers* 89 (HY2), 97–143.
1325 Clemmens, A.J., Fangmeier, D.D., 1978. Border-irrigation hydrau-
1326 lics with zero inertia—discussion. *Journal of the Irrigation and*
1327 *Drainage Division-ASCE* 104 (3), 337–339.
1328 Delis, A.I., Skeels, C.P., 1998. TVD schemes for open channel flow.
1329 *International Journal for Numerical Methods in Fluids* 26 (7),
1330 791–809.
1331 Dick, G.S., Anderson, R.A., Sampson, D.E., 1997. Controls on flash
1332 flood magnitude and hydrograph shape, Upper Blue Hills
1333 badlands, Utah. *Geology* 25 (1), 45–48.
1334 Dholakia, M., Misra, R., Zaman, M.S., 1998. Simulation of border
1335 irrigation system using explicit MacCormack finite difference
1336 method. *Agricultural Water Management* 36 (3), 181–200.
1337 Dunkerley, D., Brown, K., 1999. Flow behaviour, suspended
1338 sediment transport and transmission losses in a small (sub-
1339 bank-full) flow event in an Australian desert stream. *Hydro-*
1340 *logical Processes* 13 (11), 1577–1588.
1341 El-Hames, A.S., Richards, K.S., 1998. An integrated, physically
1342 based model for arid region flash flood prediction capable of
1343 simulating dynamic transmission loss. *Hydrological Processes*
1344 12, 1219–1232.
1345 Freyberg, D.L., 1983. Modeling the effects of a time-dependent
1346 wetted perimeter on infiltration from ephemeral channels. *Water*
1347 *Resources Research* 19 (2), 559–566.

- 1345 Garcia-Navarro, P., Saviron, J.M., 1992. McCormack method for the
1346 numerical-simulation of one-dimensional discontinuous
1347 unsteady open channel flow. *Journal of Hydraulic Research* 30
1348 (1), 95–105.
- 1349 Garcia-Navarro, P., Frías, A., Villanueva, I., 1999. Dam-break flow
1350 simulation: some results for one-dimensional models of real
1351 cases. *Journal of Hydrology* 216 (3–4), 227–247.
- 1352 Goodrich, D.C., Lane, L.J., Shillito, R.M., Miller, S.N., Syed, K.H.,
1353 Woolheiser, D.A., 1997. Linearity of basin response as a
1354 function of scale in a semiarid watershed. *Water Resources
1355 Research* 33 (12), 2951–2965.
- 1356 Goodrich, D.C., Williams, D.G., Unkrich, C.L., Hogan, J.F., Scott,
1357 R.L., Hultine, K.R., Pool, D., Coes, A.L., Miller, S., 2004.
1358 Comparison of methods to estimate ephemeral channel
1359 recharge, Walnut Gulch, San Pedro River Basin, Arizona. In:
1360 Phillips, F.M., Hogan, J.F., Scanlon, B. (Eds.), *Groundwater
1361 Recharge in a Desert Environment: the Southwestern United
1362 States*. American Geophysical Union, Washington D.C., pp. 77–
1363 99.
- 1364 Guzman, A.G., Wilson, L.G., Neuman, S.P., Osborn, M.D., 1989.
1365 Simulating effect of channel changes on stream infiltration.
1366 *Journal of Hydraulic Engineering-ASCE* 115 (12), 1631–1645.
- 1367 Henderson, F.M., 1966. *Open Channel Flow*. Macmillan, New
1368 York, NY. 522 pp.
- 1369 Izbicki, J.A., 2002. Geologic and hydrologic controls on the
1370 movement of water through a thick, heterogeneous unsaturated
1371 zone underlying an intermittent stream in the western Mojave
1372 Desert, southern California. *Water Resources Research* 38 (3)
1373 (10.1029/2000WRR000197).
- 1374 Keppel, R.V., Renard, K.G., 1962. Transmission losses in
1375 ephemeral stream beds. *Journal of Hydraulic Division, ASCE*
1376 88 (3), 59–68.
- 1377 Knighton, D., 1998. *Fluvial Forms and Processes, A New
1378 Perspective*. Arnold, London.
- 1379 Lane, L.J., 1983. Transmission losses, in: *SCS National Engineer-
1380 ing Handbook*. U.S. Government Print. Off., Washington, DC,
1381 pp. 19-1–19-21.
- 1382 Laronne, J.B., Reid, I., 1993. Very high rates of bedload sediment
1383 transport by Ephemeral Desert Rivers. *Nature* 366 (6451), 148–
1384 150.
- 1385 Leopold, L.B., Miller, J.P., 1956. Ephemeral streams-hydraulic
1386 factors and their relation to the drainage net, U.S. Geological
1387 Survey.
- 1388 Malmon, D.V., Reneau, S.L., Dunne, T., 2004. Sediment sorting
1389 and transport by flash floods. *Journal of Geophysical
1390 Research-Earth Surface* 109 (F02005) (doi:
1391 10.1029/2003JF000067).
- 1392 Osborn, H.B., Lane, L.J., 1969. Precipitation-runoff relationships
1393 for very small semiarid range watersheds. *Water Resources
1394 Research* 5 (2), 455–464.
- 1395 Parissopoulos, G.A., Wheater, H.S., 1991. Effects of wadi flood
1396 hydrograph characteristics on infiltration. *Journal of Hydrology*
1397 126, 247–263.
- 1398 Pilgrim, D.H., 1976. Travel times and nonlinearity of flood runoff
1399 from tracer measurements on a small watershed. *Water
1400 Resources Research* 12 (3), 487–496.
- 1401 Sakkas, J.G., Bellos, C.V., Klonaraki, M.N., 1994. Numerical
1402 computation of surface irrigation. *Irrigation Science* 15 (2–3),
1403 83–90.
- 1404 Sharon, D., Kutiel, H., 1986. The distribution of rainfall intensity in
1405 Israel, its regional and seasonal-variations and its climatological
1406 evaluation. *Journal of Climatology* 6 (3), 277–291.
- 1407 Shentsis, I., 2003. Increasing transmission losses from flood events
1408 due to groundwater extraction. *Hydrological Processes* 17 (4),
1409 713–725.
- 1410 Shentsis, I., Rosenthal, E., 2003. Recharge of aquifers by flood
1411 events in an arid region. *Hydrological Processes* 17 (4), 695–
1412 712.
- 1413 Shentsis, I., Meirovich, L., Ben-Zvi, A., Rosenthal, E., 1999.
1414 Assessment of transmission losses and groundwater recharge
1415 from runoff events in a wadi under shortage of data on lateral
1416 inflow, Negev, Israel. *Hydrological Processes* 13, 1649–1663.
- 1417 Sherman, B., Singh, V.P., 1982. A kinematic model for surface
1418 irrigation—an extension. *Water Resources Research* 18 (3),
1419 659–667.
- 1420 Smith, R.E., Goodrich, D.C., Woolheiser, D.A., Unkrich, C.L.,
1421 1995. KINEROS-A kinematic runoff and erosion model. In:
1422 Singh, V.J. (Ed.), *Computer Models in Watershed Hydrology*.
1423 Water Resources Publications, Highlands Ranch, CO, pp. 697–
1424 732.
- 1425 Sorman, A.U., Abdulrazzak, M.J., 1993. Infiltration-recharge
1426 through wadi beds in arid regions. *Hydrological Sciences
1427 Journal-Journal Des Sciences Hydrologiques* 38 (3), 173–186.
- 1428 Strelkoff, T., Katopodes, N.D., 1977. Border-irrigation hydraulics
1429 with zero inertia. *Journal of the Irrigation and Drainage
1430 Division-Asce* 103 (3), 325–342.
- 1431 Tabuada, M.A., Rego, Z.J.C., Vachaud, G., Pereira, L.S., 1995.
1432 Modeling of furrow irrigation—advance with 2-dimensional
1433 infiltration. *Agricultural Water Management* 28 (3), 201–221.
- 1434 van Genuchten, M.Th., 1980. A closed-form equation for predicting
1435 the hydraulic conductivity of unsaturated soils. *Soil Science
1436 Society of America Journal* 44, 892–898.
- 1437 Vanleer, B., 1979. Towards the ultimate conservative difference
1438 scheme .5. 2nd- order sequel to godunovs method. *Journal of
1439 Computational Physics* 32 (1), 101–136.
- 1440